A&A 386, 535–547 (2002)
DOI: 10.1051/0004-6361:20020238

Astronomy & Astrophysics

On the spectral evolution of Cygnus X–2 along its color-color diagram

T. Di Salvo[1], R. Farinelli[2], L. Burderi[3], F. Frontera[2,4], E. Kuulkers[5,6], N. Masetti[4], N. R. Robba[7], L. Stella[3], and M. van der Klis[1]

[1] Astronomical Institute "Anton Pannekoek", University of Amsterdam and Center for High-Energy Astrophysics, Kruislaan 403, 1098 SJ Amsterdam, The Netherlands
[2] Physics Department, University of Ferrara, Via Paradiso 12, 44100 Ferrara, Italy
[3] Osservatorio Astronomico di Roma, Via Frascati 33, 00040 Monteporzio Catone (Roma), Italy
[4] Istituto TESRE, CNR, Via P. Gobetti 101, 40129 Bologna, Italy
[5] SRON National Institute for Space Research, Sorbonnelaan 2, 3584 CA Utrecht, The Netherlands
[6] Astronomical Institute, Utrecht University, PO Box 80000, 3508 TA Utrecht, The Netherlands
[7] Dipartimento di Scienze Fisiche ed Astronomiche, Università di Palermo, via Archirafi 36, 90123 Palermo, Italy

Received 21 November 2001 / Accepted 12 February 2002

Abstract. We report on the results of a broad band (0.1–200 keV) spectral study of Cyg X–2 using two BeppoSAX observations taken in 1996 and 1997, respectively, for a total effective on-source time of ∼100 ks. The color-color (CD) and hardness-intensity (HID) diagrams show that the source was in the horizontal branch (HB) and normal branch (NB) during the 1996 and 1997 observation, respectively. Five spectra were selected around different positions of the source in the CD/HID, two in the HB and three in the NB. These spectra are fit to a model consisting of a disk blackbody, a Comptonization component, and two Gaussian emission lines at ∼1 keV and ∼6.6 keV, respectively. The addition of a hard power-law tail with photon index ∼2, contributing ∼1.5% of the source luminosity, improves the fit of the spectra in the HB. We interpret the soft component as the emission from the inner accretion disk, with inner temperature, $kT_{\rm in}$, varying between ∼0.8 and ∼1.7 keV and inner radius, $R_{\rm in}$, varying between ∼26 and ∼11 km (assuming an inclination angle of the system of 60°). The Comptonization component is probably emitted by hot plasma (electron temperature $kT_{\rm e}$ varying between ∼3 and ∼20 keV, optical depth $\tau \sim 11-0.4$, seed-photon temperature $kT_{\rm W} \sim 1-2.4$ keV) surrounding the NS. The changes in the parameters of the blackbody component indicate that the inner rim of the disk approaches the NS surface when the source moves from the HB to the NB, i.e. as the (inferred) mass accretion rate increases. The parameters of the Comptonized component also change significantly when the source moves from the HB to the NB. We discuss possible scenarios which can explain these changes.

Key words. accretion, accretion disks – stars: individual: Cyg X–2 – stars: neutron – X-rays: stars – X-rays: binaries – X-rays: general

1. Introduction

Low Mass X-ray Binaries (hereafter LMXB) are binary systems where a low-mass star loses mass which is accreted, at least in part, onto a weakly magnetic neutron star (NS) or a black hole candidate (BHC). LMXB containing NSs are usually divided into two classes: the so-called Z sources, with luminosities close to the Eddington luminosity, $L_{\rm edd}$, and the Atoll sources, which usually have lower luminosities, ∼0.01–0.1 $L_{\rm edd}$. This widely used classification relies upon a combination of the X-ray spectral properties of these sources, namely the pattern traced out by individual sources in an X-ray color-color diagram (CD) or hardness-intensity diagram (HID), and their correlated timing properties (Hasinger & van der Klis 1989). The six known (Galactic) Z sources describe a Z-track in the CD on timescales of a few days, while the sources of the atoll class trace out an atoll-shaped track in the CD on a timescale of weeks. Considerable evidence has been found that the mass accretion rate of individual Z-sources increases from the top left to the bottom right of the Z-pattern (e.g. Hasinger et al. 1990), i.e. along the so called horizontal, normal and flaring branches (hereafter HB, NB and FB, respectively). Similarly, in atoll sources the accretion rate increases from the so-called island state to the upper banana branch.

Send offprint requests to: T. Di Salvo,
e-mail: disalvo@astro.uva.nl

Accurate timing studies, mainly performed with the large area Proportional Counter Array (PCA) on board the RXTE satellite, have shown the existence of compelling correlations between rapid variability phenomena – such as Quasi-Periodic Oscillations, QPOs, band-limited noise, etc., present in the frequency range extending from Hz to kHz – and spectral states as defined by the position of the source on the CD (cf. Hasinger & van der Klis 1989; for reviews see van der Klis 1995, 2000). In fact (almost) all the timing features characterizing the power density spectra of these sources seem to vary in a smooth and monotonic way when the source moves along its CD track (e.g. Wijnands & van der Klis 1999; Psaltis et al. 1999); this clearly indicates a tight correlation between spectral and temporal behavior. These results have strengthened the idea that a single basic parameter determines both the temporal and the spectral behavior of these sources, and that this is most probably the mass accretion rate. However, the lack of a direct correlation between X-ray luminosity (where most of the accretion energy should be released) and the *inferred* mass accretion rate (e.g. Hasinger & van der Klis 1989; Méndez 2000, and references therein), is still to be understood. Indeed the observed X-ray flux may be easily affected by geometrical effects. In this case multiwavelength observations, from X-rays to UV and optical (which are thought to originate from X-rays reprocessed by the accretion disk, which subtends a large solid angle as seen from the X-ray source and is therefore less affected by geometrical effects), are required to properly study the influx of X-rays and therefore the accretion rate onto the compact object. Multiwavelength observations conducted on some Z sources have already shown a good correlation between X-ray spectral states and UV emission, indicating that the mass accretion rate increases from the HB to the NB and to the FB (see e.g. Hasinger et al. 1990; Vrtilek et al. 1990, 1991a). Alternatively, the mass accretion rate might vary non-monotonically along the CD track, a possibility suggested by some recent results, such as the decrease of the frequency of the so-called horizontal branch oscillations, HBOs, in GX 17+2 when the source was in the NB, i.e. at high inferred mass accretion rates, while simultaneously the frequency of the kHz QPOs, which are thought to track the inner radius of the disk, continued increasing (Homan et al. 2002). Also, in some cases, the X-ray burst properties, which are expected to depend on the mass accretion rate, do not show a clear correlation with the position in the CD (see e.g. Kuulkers et al. 2002). A possible explanation for this phenomenology, where the X-ray flux can directly reflect accretion rate, $\dot{M}$, and the spectral and temporal properties depend on $\dot{M}$ normalized by its own long-term average, which determines the inner radius of the disk, was recently proposed by van der Klis (2001).

The X-ray spectra (and also timing properties) of the atoll sources show some similarity with those of BHCs in their lower luminosity states. In fact these spectra can often be described by a soft component, fitted by a blackbody or a multi-temperature disk blackbody ($kT \sim 0.5{-}1$ keV), plus a power law with high energy cutoff usually at energies between ∼10 and ∼100 keV, probably originating from thermal Comptonization of soft photons by hot electrons in a surrounding corona (see, however, Markoff et al. 2001). Also, atoll sources can be found in soft (high luminosity) spectral states, where most of the energy is emitted below ∼10 keV, and hard (low luminosity) spectral states, where the soft emission is much reduced and the spectrum is dominated at high energies by a power law. It was originally thought that the electron temperature in the scattering cloud should be lower for the NSs than for the BHCs because of the extra cooling due to the soft photons emitted by the NS surface (e.g. Churazov et al. 1997). This seems indeed true for those systems in which a high energy cutoff has been observed, although some LMXBs harboring a NS do not show any evidence for a cutoff up to energies of ≥100 keV (Barret et al. 1991; Yoshida et al. 1993; Harmon et al. 1996; Piraino et al. 1999; Barret et al. 2000).

The high energy spectral hardness of LMXBs, i.e. the ratio of the count rate in the 40–80 keV band to that in the 13–25 keV band, decreases monotonically for sources of increasing luminosity (van Paradijs & van der Klis 1994). In fact the X-ray spectra of the Z sources are softer than those of atoll sources and dominated by thermal-like components with temperatures well below ∼10 keV. This is in agreement with the expectation that in a high-luminosity regime the presence of numerous soft photons could provide strong Compton cooling and result in softer spectra.

However, hard power-law components, dominating the spectrum above ∼30 keV, have been detected in several luminous and otherwise soft Z sources. These were detected several times in the past, e.g. in Sco X–1 (e.g. Peterson & Jacobson 1966), and in GX 5–1, where the power-law intensity decreased when the source moved from the NB to the FB, i.e., from lower to higher inferred mass accretion rates (Asai et al. 1994; note that contamination from a nearby source could not be excluded in this case). Hard power-law tails have been recently found in several other bright LMXBs. These components can be fit by a power law, with photon index in the range 1.9–3.3, contributing from 1% to 10% of the source luminosity; significant variations with the spectral state of the source have been detected. In particular, the first unambiguous detection of a hard tail varying with the position of the source in the CD was obtained through a 0.1–200 keV BeppoSAX observation of GX 17+2 (Di Salvo et al. 2000), where a hard power-law component was observed in the HB, which systematically weakened (by up to a factor of ∼20) when the source moved to the NB. The presence of a variable hard tail in Sco X–1 was confirmed by OSSE and RXTE observations (Strickman & Barret 2000; D'Amico et al. 2001). A hard tail was also detected in BeppoSAX data of GX 349+2 (Di Salvo et al. 2001), Cyg X–2 (Frontera et al. 1998), and the peculiar LMXB Cir X–1 (Iaria et al. 2001). In most of the cases cited above the hard component appeared to become weaker at higher inferred accretion rates. The only known exception to this behavior is

currently Sco X–1, where the presence and intensity of the hard power-law tail does not show any clear correlation with the position of the source in the CD (D'Amico et al. 2001); it might, however, be correlated with periods of radio flaring (Strickman & Barret 2000).

Among the Z sources Cyg X–2 is one of the most interesting and best-studied sources. The distance and the inclination angle of the source have been estimated to be 8 kpc and 60°, respectively (see e.g. Hjellming et al. 1990; Orosz & Kuulkers 1999). The companion is an evolved, late-type ∼0.4–0.7 $M_{\odot}$ star, the spectral type of which seems to vary from A5 to F2 with the binary period of 9.84 days, probably due to the heating of the companion surface by the X-ray emission from the compact object (see, however, Casares et al. 1998). The latter was identified as a low magnetic field NS after the observation of type-I X-ray bursts from the system (e.g. Kahn & Grindlay 1984). Cyg X–2 shows high-intensity states (with a 2–10 keV luminosity higher than 7×10^{37} ergs/s), usually characterized by irregular dipping activity (Vrtilek et al. 1988; see also Kuulkers et al. 1996). This dipping activity is absent during the low-intensity states, which instead show a modulation of the X-ray flux, i.e. an intensity reduction up to 40% at the binary phase 0.4–0.8, probably due to the obscuration of an accretion disk corona by a tilted accretion disk (Vrtilek et al. 1988). Cyg X–2 usually exhibits all three branches of the Z-track, although its behavior in the FB is quite unusual. It shows an intensity decrease from the bottom of the NB to the FB which can be identified with the dipping activity. Cyg X–2, together with GX 5–1 and GX 340+0, shows secular variations of the position of the Z-pattern in the CD on long time scales (more than a few days; see Kuulkers et al. 1996 for an extensive study). These variations have been interpreted in terms of a high inclination angle of these sources, allowing matter near the equatorial plane to modify the emission from the central region (e.g. Kuulkers et al. 1996), but these could also be a consequence of a more general behavior of LMXB accretion (van der Klis 2001). Simultaneous multiwavelength observations showed that the UV flux and optical emission lines' strength increase from the HB to the FB (Vrtilek et al. 1990; van Paradijs et al. 1990). Also, strong non-thermal radio flares were observed in the HB and upper NB, whereas the source was radio quiet in the lower NB and in the FB (Hasinger et al. 1990).

The continuum spectrum of Cyg X–2 has been fitted by two-component models, in particular the so-called Western model (White et al. 1986), consisting of a blackbody component, originating from (or close to) the NS, and a power law with high energy cutoff, approximating unsaturated Comptonization from the inner disk (see e.g. Hasinger et al. 1990 using Ginga data; Smale et al. 1993 using BBXRT data), and the Eastern model (Mitsuda et al. 1984), consisting of a multi-temperature blackbody from the accretion disk and a Comptonized blackbody from the NS (e.g. Hasinger et al. 1990; Hoshi & Mitsuda 1991 using Ginga data). In the framework of the Eastern model, the disk emission has also been described by non-standard models, where the radial temperature gradient q was considered as a free parameter in the fit (Hirano et al. 1995). This parameter was found to change continuously from the HB to the FB, suggesting that the disk undergoes structural changes when the source moves along the CD. However, the evolution of the spectral parameters of the source along the CD track is still not clear, given that the data collected and examined up to now did not allow distinguishing between the different models, which in turn led to different results (for recent results see Piraino et al. 2002; Done et al. 2002). The Cyg X–2 X-ray spectrum above ∼20 keV has been studied with detectors on balloons (an overview of the earliest high energy observations of Cyg X–2 can be found in Peterson 1973). Interestingly, an unexpectedly hard spectrum was observed from Cyg X–2. This was fitted by a power law with photon index 2.8 (Maurer et al. 1982) or 1.9 (Ling et al. 1996). Matt et al. (1990) concluded that, while the 25–50 keV flux from Cyg X–2 was compatible with the extrapolation of the low energy spectrum, the shape of the hard spectrum was flatter than expected, and that therefore only simultaneous broad band observations of the X-ray spectrum could confirm or disprove the presence of a third hard component.

An emission line at ∼6.7 keV from highly ionized iron has also been reported in the energy spectrum. The line is quite broad (its width was measured from BBXRT data to be ∼1 keV *FWHM*) and has an equivalent width of ∼60 eV (Smale et al. 1993). These authors suggest that the width of the line, together with the lack of a significant iron absorption edge, could be explained by reflection from a highly ionized disk surface. An Fe absorption edge, with an energy of 8 keV and column density of $\sim10^{19}$ cm^{-2}, was reported in the lower NB and in the FB from Ginga observations (Hirano et al. 1995). Note, however, that these features are usually quite broad and therefore sensitive to the assumed continuum model. Emission lines at energies between 0.6−1.1 keV were reported several times (see e.g. Vrtilek et al. 1986, 1991b; Kuulkers et al. 1997); these likely result from ionized O and Fe. The strength and energy of these soft lines appears to depend on the spectral state of the source. This is to be expected given that these lines are very sensitive to the temperature of the emitting material (Kallman et al. 1989).

We report here on the broad band (0.1–200 keV) spectral analysis of two BeppoSAX observations of Cyg X–2. The source was in the HB and NB during these observations, providing the possibility of studying the spectral variations along a considerable part of the CD. A hard power-law tail is significantly detected only in the HB spectra, showing a behavior similar to that observed in GX 17+2.

2. Observations

We analyzed two BeppoSAX (Boella et al. 1997) observations of Cyg X–2 from the public BeppoSAX archive. The first observation was performed during the Science

Verification Phase (SVP) on 1996 July 23 for an exposure time of ∼33 ks. The second observation took place in 1997 October 26–28, for an exposure time of ∼66 ks. Results from the 1996 and 1997 observations were discussed, respectively, in Kuulkers et al. (1997, who analyzed the 0.1–10 keV spectrum from the low-energy instrument) and in Frontera et al. (1998, who analyzed the 2–200 keV spectrum, averaged over the whole observation). The BeppoSAX Narrow Field Instruments (NFI) consist of four co-aligned instruments covering the energy range between 0.1 and 200 keV. X-ray images were obtained with three (in July 1996) and two (in October 1997) Medium Energy Concentrator Spectrometers (MECS, position sensitive gas scintillator proportional counters operating in the 1.3–10.5 keV band; Boella et al. 1997; in May 1997 detector unit 1 stopped working) and a Low Energy Concentrator Spectrometer (LECS, a thin-window position-sensitive gas scintillator proportional counter with extended low energy response, 0.1–10 keV; Parmar et al. 1997), each in the focal plane of the X-ray concentrators. These in turn consist of a set of 30 nested conical mirror shells providing an approximation to a Wolter-I type geometry. Due to UV contamination problems, the LECS was operated only at satellite night time, resulting in reduced exposure time (∼10.2 and ∼23 ks for the 1996 and 1997 observations, respectively). The LECS and MECS Cyg X–2 data were extracted from circular regions centered on the source and with radii of $8'$ and $4'$, respectively, corresponding to ∼90% of the instruments' point spread function. Data extracted from the same detector regions during blank field observations were used for background subtraction. The High Pressure Gas Scintillation Proportional Counter (HPGSPC; energy range of 6–30 keV; Manzo et al. 1997) and Phoswich Detection System (PDS; energy range of 13–200 keV; Frontera et al. 1997) are non-imaging instruments, the field of view (∼1° *FWHM*) of which is limited by rocking collimators that can alternate on and off the source. Background subtraction for these instruments was obtained from data accumulated during off-source intervals. The effective exposure was 20 and 26 ks in the HPGSPC and 18 and 27 ks in the PDS during the 1996 and 1997 observations, respectively. No contaminating sources are known to be present within 1° from Cyg X–2, and all the available evidences confirm that there were no significant contaminating sources in the field of view of the HPGSPC and PDS, both in the on-source and off-source positions. In fact the off-source count rates are in the expected range and display the characteristic orbital dependence arising from the variable particle background; moreover the HPGSPC and PDS spectra align well with each other and with the MECS spectra.

The light curve of Cyg X–2 in the MECS energy range (1.4–10.5 keV) during the 1996 and 1997 observation is shown in Fig. 1 (left and right panel, respectively). During the 1996 observation the intensity gradually increased from ∼120 to ∼180 counts/s, while during the 1997 observation it was quite constant at ∼190 counts/s, except for a "dip" in the first part of the observation, during which the intensity decreased to ∼160 counts/s. Figure 2 shows the CD (left) and the HID (right) where the hard color, HC, is the ratio of the 7–10.5 keV and 4.5–7 keV MECS count rates, the soft color, SC, is the ratio of the 4.5–7 keV and 1.4–4.5 keV MECS count rates and the intensity is again the 1.4–10.5 keV count rate. Two branches are clearly seen in the diagrams, closely resembling the HB and NB, due to, respectively, the 1996 and 1997 data. The two branches seem to connect in the usual way, so there are no obvious shifts in the CD or HID. Note that the source intensity variations in the HB were relatively pronounced. The 1996 observation was therefore divided into two intervals, corresponding to different source intensity ranges, as indicated in Fig. 2 (right panel). We will refer to these two intervals as the upper HB (i.e. the interval corresponding to the lower intensity range in the HB) and the lower HB (the interval corresponding to the higher intensity level in the HB). During the 1997 observation the source was in the NB, and larger changes in the colors took place, while the variations in intensity were less pronounced. This observation was divided into three time intervals, in which the source, on the average, exhibited different SC, even if on short time scales the behavior of the SC was more complex. These intervals are shown in Fig. 2 (left panel). We call these intervals lower NB (corresponding to lower SC values in the NB), middle NB (corresponding to intermediate SC values in the NB) and upper NB (corresponding to higher SC values in the NB). In order to investigate the changes of the source spectrum as a function of position in the CD or HID, we accumulated the energy spectra of each NFI over the five different intervals described above, i.e. two spectra in the HB and three in the NB. The (absorbed) source luminosity in the 0.1–100 keV energy band ranged from $\sim 0.89 \times 10^{38}$ ergs/s in the upper HB to $\sim 1.5 \times 10^{38}$ ergs/s in the NB, assuming a source distance of 8 kpc.

In our spectral analysis we used data corresponding to the following energy ranges: 0.12–4 keV for the LECS, 1.8–10 keV for the MECS, 8–30 keV for the HPGSPC and 15–200 keV for the PDS. All spectra were rebinned in order to oversample the full width at half maximum of the energy resolution by a factor of 5. A systematic 1% error was added to each spectrum to account for calibration uncertainties. As customary, in the spectral fitting procedure we allowed for different normalizations in the LECS, HPGSPC and PDS spectra relative to the MECS spectra, and checked a posteriori that the derived values are in the standard range for each instrument[1].

3. Spectral analysis

In line with previous studies (e.g. Mitsuda et al. 1984; White et al. 1988; Di Salvo et al. 2000, 2001), we tried several two-component models to fit the X-ray

[1] see the BeppoSAX handbook at `ftp://sax.sdc.asi.it/pub/sax/doc/software_docs`

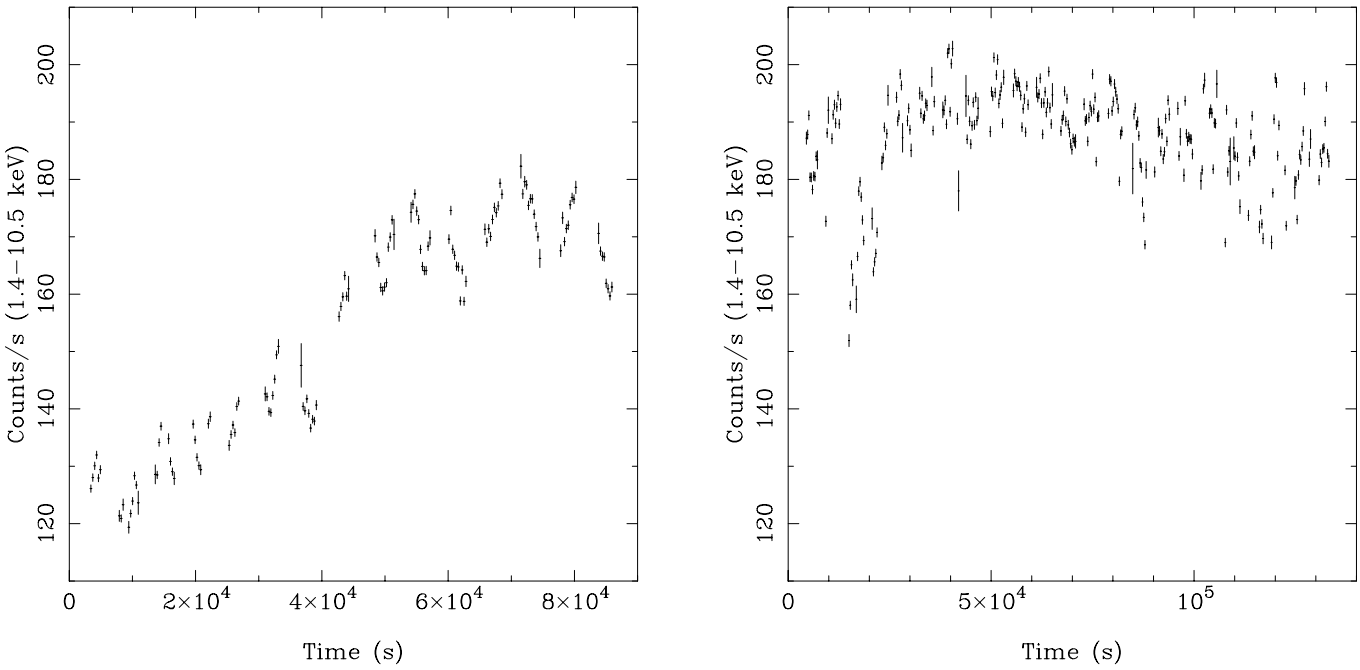

Fig. 1. Light curve of Cyg X–2 in the 1.4–10.5 keV range (MECS data) during the 1996 observation (starting time July 23 00:54:21 UT, left panel) and the 1997 observation (starting time October 26 15:37:11 UT, right panel), respectively. Each bin corresponds to 300 s integration time.

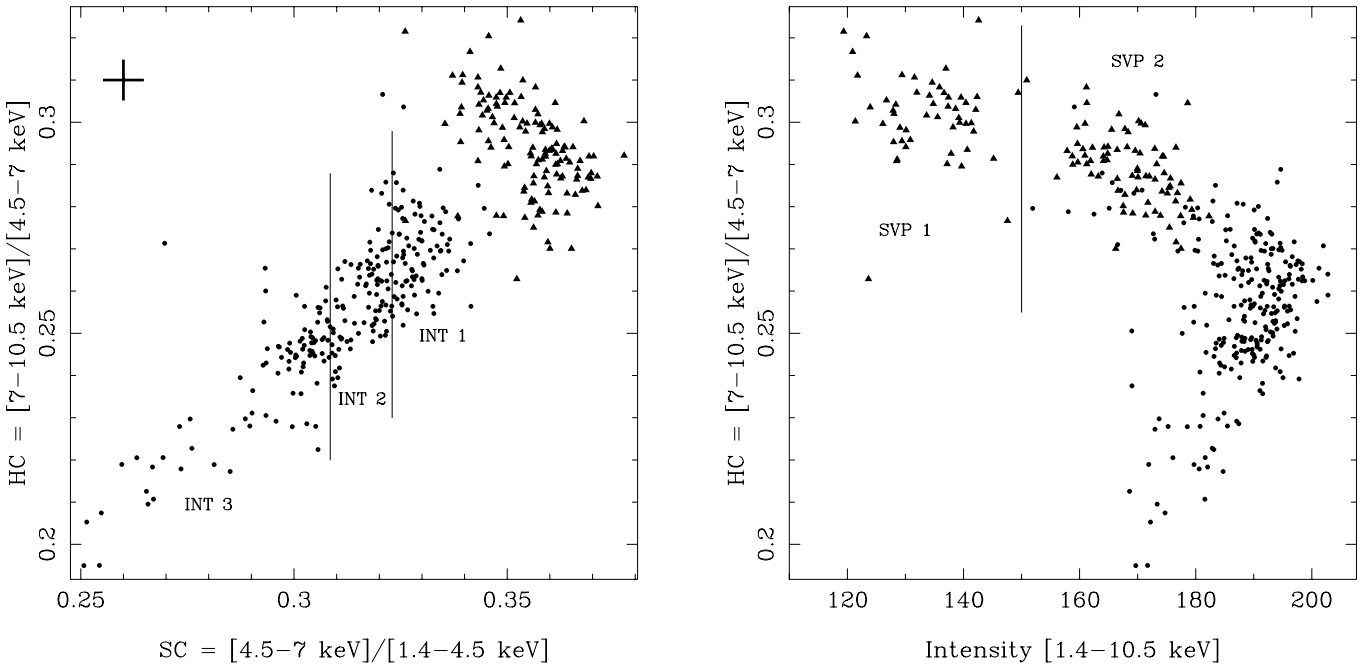

Fig. 2. Color-color diagram (left) and hardness-intensity diagram (right) of Cyg X–2 during the 1996 observation (triangles) and the 1997 observation (circles). The hard color (HC) is the ratio of the counts in the energy bands 7–10.5 keV and 4.5–7 keV, the soft color (SC) is the ratio of the counts in the energy bands 4.5–7 keV and 1.4–4.5 keV, the source intensity is the count rate in the MECS (energy range 1.4–10.5 keV). Each point corresponds to 300 s integration time. A typical error bar is shown at the top left corner of the left panel. The intervals in which the CD/HID were divided for the spectral analysis (see text) are also shown.

continuum of Cyg X–2. These were a blackbody or a multi-temperature blackbody disk model (`diskbb` in the terminology of the spectral fitting program XSPEC v.11) for the soft component, together with a blackbody or a thermal Comptonization model for the harder component. Among Comptonization spectra we considered: a power law with exponential cutoff (`cutoffpl`), a Comptonization spectrum of cool photons scattering off hot electrons (`compst`,

based on the solution of the Kompaneets equation given by Sunyaev & Titarchuk 1980), and a Comptonization spectrum of an input Wien spectrum of soft photons by a hot plasma (`comptt`, which includes relativistic effects and takes into account the dependence of the scattering opacity on seed-photon energy, which is a free parameter of the model; Titarchuk 1994; Hua & Titarchuk 1995; Titarchuk & Lyubarskij 1995).

For the three spectra in the NB the best fit to the continuum was found using the `diskbb` plus `comptt` model (see results in Table 1). This is slightly different from the blackbody plus `comptt` model that was used to fit the spectra of other Z sources (e.g. Di Salvo et al. 2000; Di Salvo et al. 2001); in the case of Cyg X–2 this model gave significantly worse fits for some of the intervals. In fact by using this model we obtained χ^2/d.o.f. of 274/190, 398/190 and 273/189 for the spectra of the upper NB, the middle NB and the lower NB, respectively, generally worse (especially in the case of the middle NB spectrum) than the results obtained using `diskbb` instead of blackbody (cf. Table 1). The fit with the `diskbb` is preferable also because using the blackbody for the soft component the low energy line becomes unphysically broad ($\sigma \sim 0.32$ keV) and strong (equivalent width of ∼230 eV) and centered at lower energies (∼0.89 keV). In the cases of the middle and the lower NB spectra the fit using the single-temperature blackbody can be improved adding a power law with photon index ∼3. This model gives χ^2/d.o.f. of 311/188 and 213/187 for the middle NB and lower NB, respectively, which are comparable with the ones obtained using `diskbb` for the soft component. Again this last model is preferable because it is simpler and because the steep power law is indeed needed to fit the soft part of the spectrum instead of the hard part, where it gives almost no contribution. We therefore assumed the `diskbb` plus `comptt` model reported in Table 1 as the best fit model.

The temperature of the disk blackbody component is ∼1.6 keV, slightly decreasing from the upper to the lower NB. The corresponding inner disk radius, $R_{\rm in}\sqrt{\cos i}$, is between 8.1 and 9.7 km, slightly increasing along the NB. The Comptonized component gives a seed-photon temperature of ∼2 keV, slightly decreasing along the NB. These photons are Comptonized by hot electrons at a temperature that seems to increase from ∼3.5 keV to ∼20 keV along the NB. At the same time the optical depth of the Comptonizing cloud (calculated in the case of a spherical geometry) decreases from ∼7 to ∼0.4. Note, however, that the uncertainty on these two parameters becomes very large in the lower-NB spectrum. We have calculated the radius, $R_{\rm W}$, of the seed-photon emitting region by using the bolometric luminosity of the soft photons obtained from the observed luminosity of the Comptonized spectrum after correction for energy gained in the inverse Compton scattering, and assuming a spherical geometry. This can be expressed as $R_{\rm W} = 3{\times}10^4 D\sqrt{\frac{f_{\rm bol}}{1+y}}/\left(kT_0\right)^2$ km (in 't Zand et al. 1999), where D is the distance to the source in kpc, $f_{\rm bol}$ is the unabsorbed flux of the Comptonization spectrum in erg cm^{-2} s^{-1}, kT_0 is the seed–photon temperature in keV, and $y = 4kT_{\rm e}\tau^2/m_{\rm e}c^2$ is the relative energy gain due to the Comptonization. Inferred radii, reported in Table 1, are in the range between 1.8 and 3.5 km. These are small when compared to the values that were obtained for GX 17+2 (with $R_{\rm W} \sim 12{-}17$ km; Di Salvo et al. 2000) and GX 349+2 ($R_{\rm W} \sim 7{-}9$ km; Di Salvo et al. 2001), by using a similar model.

We used the same continuum model to fit the spectra in the HB, although in the spectrum of the upper HB the soft component is similarly well described by a blackbody or a `diskbb` model. In fact, because the soft component has now a much lower temperature, these two models become virtually undistinguishable. The inner disk temperature is now 0.8–0.9 keV, corresponding to a larger inner disk radius of $R_{\rm in}\sqrt{\cos i} \sim 16{-}19$ km. The seed-photon temperature is around 1 keV, with a radius of the seed-photon emitting region of $R_{\rm W} \sim 10$ km. The Comptonizing cloud has an electron temperature of ∼3 keV and an optical depth of ∼10. The values of the parameters in this case are very similar to those found for GX 17+2 and GX 349+2.

However, in these spectra the PDS data points above 30 keV were systematically above the model, as it can be seen in the residuals (in units of σ) shown in Fig. 3 (middle panels). To fit these points we added a power-law component to the continuum model. The addition of this component eliminates the residuals at high energy (see Fig. 3, bottom panels), giving a reduction of the χ^2/d.o.f. from 292/195 to 270/193 for the upper HB and from 259/193 to 234/191 for the lower HB, corresponding to a probability of chance improvement (calculated using an F-test) of $\sim 4.8\times10^{-4}$ and $\sim 3.6\times10^{-4}$, respectively. Other models for this hard excess (e.g., a thermal bremsstrahlung with temperature of the order of a few tens of keV) gave comparably good results. The power-law component has a photon index of 1.8–2.1 and contributes ∼1.5% of the 0.1–100 keV observed luminosity. We tried to average together the two spectra in the HB, given that the obtained spectral parameters for these two spectra are quite similar. In this case, we could obtain a stable fit only fixing the $N_{\rm H}$ and the Fe line centroid energy. The obtained spectral parameters for the average HB spectrum are similar to those obtained for each of the two spectra. However, in this case the statistical significance of the hard power-law component is higher. The addition of this component in fact reduces the χ^2 from 466 (263 d.o.f.) to 424 (261 d.o.f.), corresponding to a probability of chance improvement of $\sim 4\times10^{-6}$.

Fixing the photon index to 2.09 (i.e. the best fit value in the lower HB), we found upper limits at 90% confidence level to the power-law normalization in the spectra of the NB, where such a component is not required. These upper limits, together with the F-test for the addition of this component, are reported in Table 1. The derived upper limits are still compatible with the best fit values of the

Table 1. Results of the fit of Cyg X–2 spectra in the energy band 0.12–200 keV, with a disk blackbody, a Comptonized spectrum modeled by `Comptt`, a power law, and two Gaussian emission lines. Uncertainties are at the 90% confidence level for a single parameter. $kT_{\rm W}$ is the temperature of the soft seed photons for the Comptonization, $kT_{\rm e}$ is the electron temperature, τ is the optical depth of the scattering cloud in a spherical geometry. I is the intensity of a Gaussian emission line in units of photons cm^{-2} s^{-1}. The power-law normalization is in units of photons keV^{-1} cm^{-2} s^{-1} at 1 keV. Upper limits on the power law normalizations are at 90% confidence level. The total flux, in units of 10^{-8} ergs cm^{-2} s^{-1}, refers to the 0.1–100 keV energy range. F-test indicates the probability of chance improvement of the fit when the power law is included in the spectral model.

Spectrum Position	SVP1 UHB	SVP2 LHB	INT1 UNB	INT2 MNB	INT3 LNB
$N_{\rm H}$ ($\times10^{22}$ cm^{-2})	0.197 (frozen)	0.197 ± 0.015	0.1904 ± 0.0029	0.1823 ± 0.0021	0.1911 ± 0.0047
$kT_{\rm in}$ (keV)	$0.82^{+0.07}_{-0.15}$	0.92 ± 0.55	1.694 ± 0.022	1.659 ± 0.019	1.546 ± 0.030
$R_{\rm in}\sqrt{\cos i}$ (km)	18.6 ± 3.5	16.1 ± 2.1	8.08 ± 0.16	8.7 ± 0.16	9.74 ± 0.30
$kT_{\rm W}$ (keV)	1.062 ± 0.12	1.12 ± 0.12	2.39 ± 0.39	2.285 ± 0.043	2.04 ± 0.11
$kT_{\rm e}$ (keV)	3.106 ± 0.056	3.018 ± 0.054	3.5 ± 1.1	$8.7^{+21}_{-1.9}$	20^{+61}_{-20}
τ	10.89 ± 0.30	10.47 ± 0.35	6.9 ± 3.0	1.53 ± 0.94	$0.43^{+3.0}_{-0.40}$
$R_{\rm W}$ (km)	9.7 ± 2.2	9.8 ± 2.1	1.83 ± 0.68	$2.77^{+0.53}_{-0.26}$	$3.56^{+0.81}_{-0.40}$
Photon Index	1.83 ± 0.37	2.09 ± 0.55	2.09 (frozen)	2.09 (frozen)	2.09 (frozen)
Power-law N	$0.015^{+0.051}_{-0.013}$	$0.040^{+0.061}_{-0.010}$	<0.027	<0.039	<0.018
$E_{\rm Fe}$ (keV)	6.6 (frozen)	6.60 ± 0.20	6.65 ± 0.11	6.698 ± 0.092	6.58 ± 0.16
$\sigma_{\rm Fe}$ (keV)	$0.31^{+0.39}_{-0.07}$	0.65 ± 0.33	0.26 ± 0.12	0.21 ± 0.17	0.59 ± 0.32
$I_{\rm Fe}$ ($\times10^{-3}$)	3.0 ± 1.6	4.9 ± 3.6	3.54 ± 0.97	3.1 ± 1.0	6.7 ± 3.2
Fe Eq. W. (eV)	42	55	28	24	55
$E_{\rm LE}$ (keV)	0.988 ± 0.041	1.064 ± 0.045	1.051 ± 0.021	1.045 ± 0.013	1.060 ± 0.024
$\sigma_{\rm LE}$ (keV)	0.196 ± 0.041	0.184 ± 0.060	0.109 ± 0.024	0.124 ± 0.020	0.108 ± 0.025
$I_{\rm LE}$ ($\times10^{-2}$)	9.4 ± 2.0	10.7 ± 2.8	5.41 ± 0.96	7.0 ± 1.1	7.7 ± 1.8
LE Eq. W. (eV)	71	80	28	33	38
Flux	1.17	1.40	1.97	2.08	1.94
$\chi^2_{\rm red}$ (d.o.f.)	1.40 (193)	1.24 (191)	1.29 (190)	1.68 (190)	1.14 (189)
F-test	4.8×10^{-4}	3.6×10^{-4}	0.16	0.019	0.78

power-law normalization in the HB, indicating that the reason for the non-detection of the power law in the NB might be the hardening of the Comptonized component, the electron temperature of which systematically increases when the source moves from the HB to the NB.

Two emission lines are needed to fit all these spectra: the first one is at an energy between 0.99 and 1.06 keV and seems to be stronger in the HB (where it is also broader), with equivalent widths of 70–80 eV, than in the NB, where the equivalent widths are between 28 and 38 eV. The second emission line is at an energy of 6.6–6.7 keV, with equivalent widths from 24 to 55 eV. Note that also in this case the equivalent width is higher when the width is larger (i.e. in the HB and lower NB, see Table 1). Both these lines are highly significant in our spectra (F-tests give probabilities of chance improvement lower than $\sim10^{-18}$ for the addition of the low-energy emission line, and lower than 7×10^{-5} for the addition of the iron Kα line) and were already known to be required to fit the spectrum of Cyg X–2 (see e.g. Kuulkers et al. 1997; Smale et al. 1993, and references therein).

Data and residuals in units of σ with respect to the corresponding best fit model containing all the required spectral components are shown in Figs. 3 and 4 (top and bottom panels, respectively) for four representative spectra. Note that for the upper-HB spectrum the fit is unstable if all parameters are set free, because of the interplay of the several spectral components to fit the low energy part of the spectrum. We obtained a stable fit by fixing the equivalent absorption column, $N_{\rm H}$, and the Fe line centroid energy to the best fit values obtained for the lower-HB spectrum. In all the other cases the fit was stable, including the lower-HB spectrum which has the same number of parameters (this can be due to the higher intensity in this interval). To better see the spectral changes in Cyg X–2 according to the model described above, we show in Fig. 5 the unfolded spectra for the interval corresponding to the lower HB and the three intervals in the NB, together with the components of the best fit model.

From an inspection of the residuals (Figs. 3 and 4, bottom panels) we can see that some structures are still present at energies lower than 5 keV, which may indicate the presence of other narrow emission/absorption features. In particular, the feature which has the highest statistical significance is an excess around 2.5 keV. Adding a Gaussian emission line at this energy gives an improvement of the fit with a probability of chance improvement between $\sim7 \times 10^{-2}$ and $\sim10^{-6}$. The highest statistical significance for the addition of this feature is found in the middle NB spectrum, where this reduces the χ^2/d.o.f. from 320/190 to 272/187. The best fit parameters of this line give a centroid energy of 2.631 ± 0.033 keV, a width $\sigma \lesssim 0.09$ keV (compatible with the instrumental energy resolution) and an intensity of $(7.3 \pm 1.8) \times 10^{-3}$

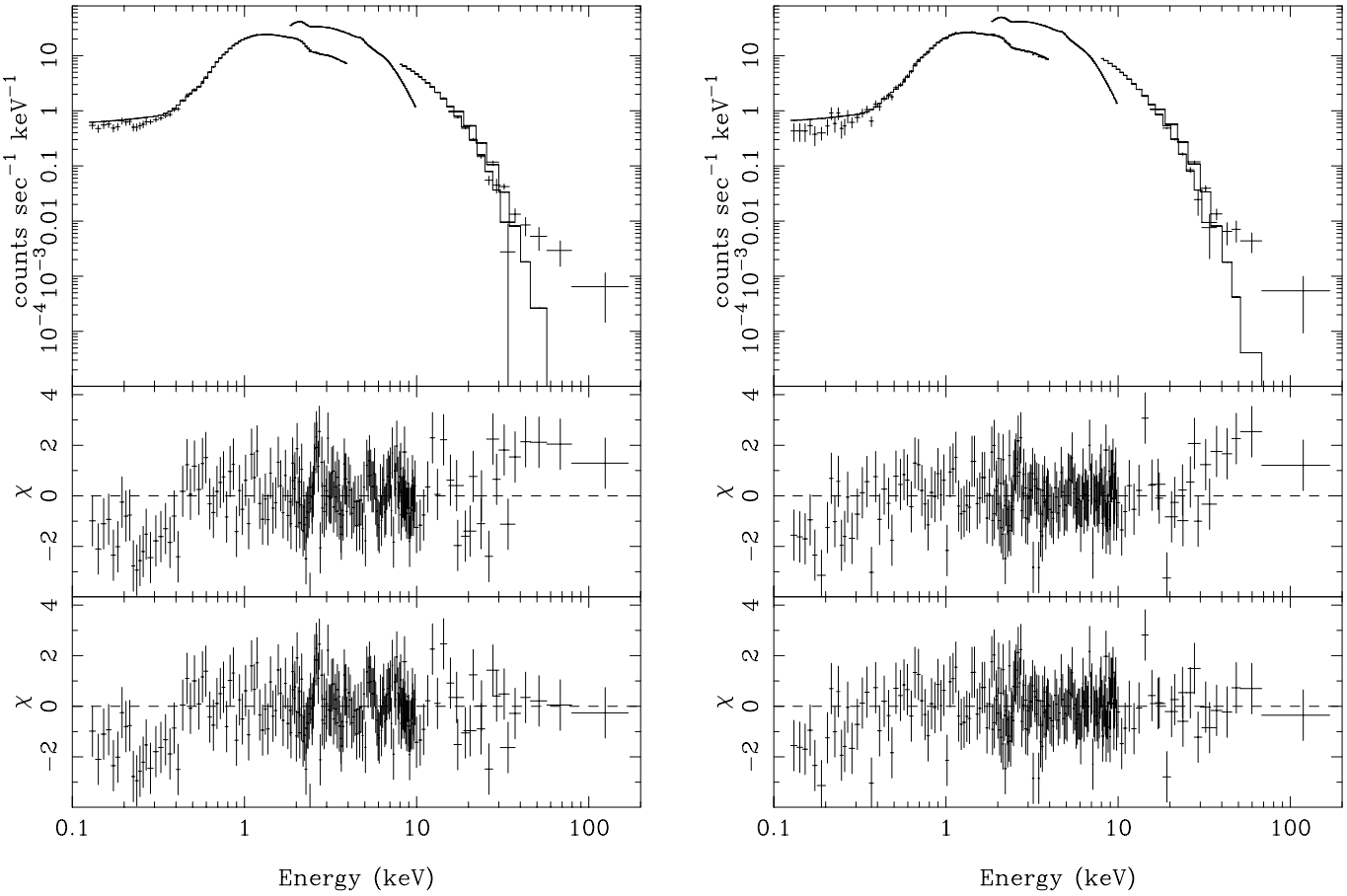

Fig. 3. The broad band spectrum of Cyg X–2 in the upper HB (left panel), and in the lower HB (right panel), respectively, together with the best fit two-component continuum model (disk blackbody plus `comptt`) are shown in the top panels, and the corresponding residuals in unit of σ are shown in the middle panels. Residuals in unit of σ with respect to the best fit model reported in Table 1, including a hard power-law component, are shown in the bottom panels.

photons cm^{-2} s^{-1}. Note that the reduced χ^2 found for the middle NB spectrum is still high to be statistically acceptable. However, the model described above is the one which gave the best fit to this spectrum and no obvious features are visible in the residuals with respect to this model. Also a high value of the χ^2 is not surprising given the high statistics of the BeppoSAX broad band spectra and the intrinsic complexity of this kind of spectra.

4. Discussion

We have analyzed two BeppoSAX observations of the LMXB and Z source Cyg X–2 carried out in 1996 and 1997, respectively, for a total exposure time of ∼100 ks. As already mentioned, Cyg X–2 is known to show complex long term intensity variations; high-intensity and low-intensity states have been observed to be characterized by quite different behaviors. Cyg X–2 also shows secular shifts of the position of the Z-track in the CD/HID. Therefore it is not straightforward to conclude whether or not the two BeppoSAX observations belong to similar states. We have identified the BeppoSAX observation periods in the RXTE/All Sky Monitor light curve. We can see that the 1996 observation occurred a few days before the transition to a probable low-intensity state, and probably corresponds to a "medium state", which sometimes has been observed (Vrtilek et al. 1986). The 1997 observation occurred during a quite high-intensity state. However, the CD and HID of these two observations connect smoothly both in the hard and soft colors and the intensity, suggesting that there are no significant shifts between the two observations, although we cannot exclude that they belong to different spectral states. The source was mainly in the HB during the 1996 observation and in the NB during the 1997 observation. We selected five spectra in different positions of the CD/HID; two of these spectra correspond to the HB and three to the NB. The 0.1–100 keV source luminosity increases from 0.89×10^{38} ergs/s to 1.5×10^{38} ergs/s (assuming a distance of 8 kpc) when the source moves from the upper HB to the lower HB and then to the upper NB. In the NB the luminosity remains almost constant at 1.5×10^{38} ergs/s.

The X-ray spectrum of Cyg X–2 has a complex shape and requires several components, which makes the spectral fitting non-unique (see also Piraino et al. 2002; Done et al. 2002). Keeping this in mind we now discuss the two-component continuum model which gave the best fit to most of the spectra analyzed here, which consists of a

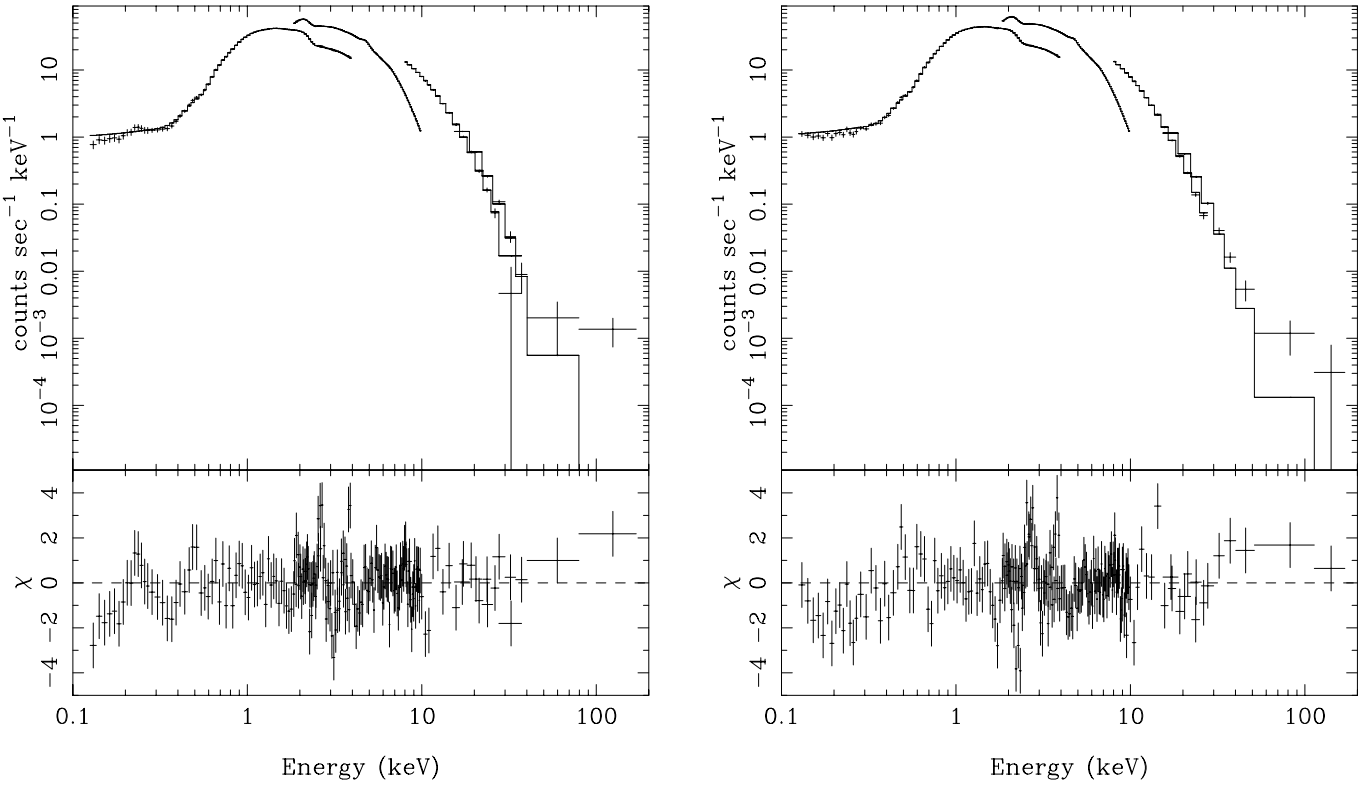

f4

Fig. 4. The broad band spectrum of Cyg X–2 in the upper NB (left panel), and in the middle NB (right panel), respectively, together with the best fit model are shown in the top panels, and the corresponding residuals in unit of σ are shown in the bottom panels.

disk blackbody plus the Comptonization model `comptt`. This is different from the continuum model that was used to describe the BeppoSAX broad band spectrum of other Z sources (GX 17+2, Di Salvo et al. 2000; GX 349+2, Di Salvo et al. 2001), i.e. a single temperature blackbody plus `comptt`. The difference might be ascribed to the higher temperature of the soft component in Cyg X–2. In fact, while in GX 17+2 and GX 349+2 the temperature of the blackbody component is in the range 0.5−0.6 keV, in Cyg X–2 this temperature is higher, ranging from ∼0.8 keV in the upper HB up to ∼1.7 keV in the NB. Note that when the temperature of the soft component is low (and close to the lower end of the instrument energy range) the disk multi-temperature blackbody and the single-temperature blackbody become indistinguishable, and in fact both these models can well fit the Cyg X–2 spectrum in the upper HB, where the temperature of the soft component is the lowest. On the other hand, when the temperature of the soft component is high (and far from the lower end of the energy range) the difference between the simple blackbody and the disk blackbody (the low-energy end of which is considerably flatter) becomes important, and it is possible to discriminate between these models. This leads us to interpret the soft component in all these spectra as the emission from the inner accretion disk, in agreement with the so-called Eastern model (Mitsuda et al. 1984). This interpretation is in agreement with the results obtained from the spectral analysis of type-I X-ray bursts from GX 17+2 (Kuulkers et al. 2002). In that case the soft component in the persistent emission remains constant during the bursts, thus suggesting that it does not come from the NS.

Also the Cyg X–2 spectra show that the inner disk temperature significantly increases (from ∼0.8 keV to ∼1.7 keV) when the source moves from the HB to the NB, indicating that the inner rim of the disk approaches the NS at higher inferred mass accretion rates. In fact the inner disk radius, $R_{\rm in}$, obtained from these spectra decreases from ∼26 km in the upper HB to ∼11.5 km in the upper NB, assuming an inclination angle $i = 60°$. Note that we are here neglecting the systematics effects affecting the values of the inner disk inferred from the `diskbb` model, such as the color temperature correction (e.g. Shimura & Takahara 1995), relativistic effects (e.g. Zhang et al. 1997) and the effect of the stress-free inner boundary condition (e.g. Frank et al. 1992), which usually tend to increase the inferred inner radii by a factor of the order of 1.5−2. However, the behavior of the inner disk radius is at least qualitatively in agreement with the observed behavior of the frequencies of the kHz QPOs as a function of the position in the CD. Two kHz QPOs were simultaneously observed in Cyg X–2, at ∼500 and ∼860 Hz, respectively (Wijnands et al. 1998). The frequency of the upper peak systematically increases when the source moves down the HB, reaching a maximum of ∼1 kHz in the upper NB, before disappearing. As a

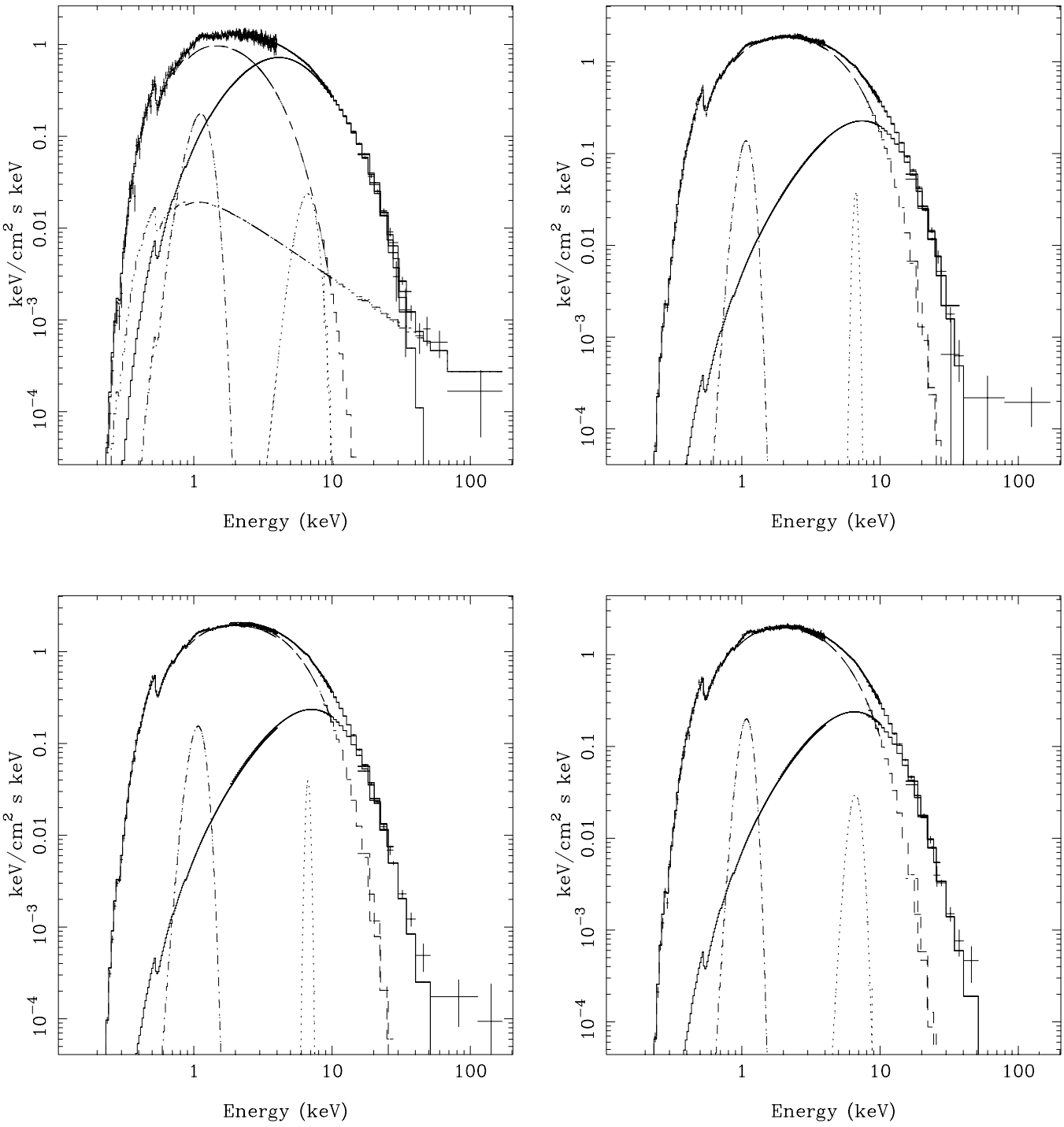

Fig. 5. Unfolded spectra of Cyg X–2 in the lower HB (top left), upper NB (top right), middle NB (bottom left), and lower NB (bottom right). The best fit models reported in Table 1 are shown in this figure as the solid lines on top of the data. The individual model components are also shown, namely the disk blackbody (dashed line), the Comptonized spectrum (`comptt` model, solid line), two Gaussian emission lines, one at ∼1 keV (dot-dashed line) and the other at ∼6.7 keV (dotted line), and the power-law (when significantly detected, dot-dot-dot-dashed line).

consistency check we can derive the NS mass from these independent measurements. Assuming that the lowest and highest frequencies measured for the upper kHz QPO (∼730 Hz and ∼1000 Hz, respectively) correspond, respectively, to the Keplerian frequency at the largest and smallest disk inner radius measured here, we can calculate the NS mass from the Keplerian law: $M = \nu^2 R_{\rm in}^3 4\pi^2/G$. This gives $M \simeq (2.8 \pm 1.6) M_\odot$ and $M \simeq (0.45 \pm 0.03) M_\odot$, respectively, which are within a factor of 3 from the standard NS mass of 1.4 $M_\odot$. These are not unreasonable values considering the uncertainties in the disk model and in the correspondence between the kHz QPO frequencies and

disk inner radii, which are not measured simultaneously in this case (note that the errors on the inferred mass are derived considering only the uncertainties on the best fit values of the inner disk radius). In particular the radius in the NB is probably underestimated, but this is not surprising given that the correction factors mentioned above are expected to be higher when the radius becomes smaller. Therefore the uncertainties are too large, at the moment, to allow us to prove or disprove the assumed model.

This behavior, however, is different from that of GX 17+2 for which the parameters of the soft component seem to remain almost constant along the HB and NB (Di Salvo et al. 2000). This can also be deduced from the shape of the CD of this source, where the HB and NB appear to be almost vertical (with SC on the x-axis; see Wijnands et al. 1997), indicating that only small variations occur in the SC. In other words, in this scenario it is not clear why GX 17+2 does not show a variation of the soft component similar to the one observed for Cyg X–2, although it shows a similar behavior of the kHz QPO frequencies (see Wijnands et al. 1997; Homan et al. 2002). This different behavior of the inner part of the disk might also have been observed in UV. Indeed UV observations of Sco X–1 (note that GX 17+2 is a Sco-like source, see below) show that the disk structure does not change when the source moves along the CD (Vrtilek et al. 1991). On the other hand UV observations of Cyg X–2 show that while the outer disk structure remains unchanged, the inner disk (shorter UV wavelengths) varies when the source moves along the CD (S. D. Vrtilek 2001, private comm.).

Other significant changes at the transition between the HB and NB occur in the parameters of the Comptonization component produced by the upscattering of soft seed photons by hot electrons. In particular, the seed-photon temperature increases from ∼1 keV to ∼2.4 keV when the source moves from the HB to the NB. At the same time the electron temperature of the Comptonizing plasma systematically increases and the optical depth systematically decreases. The radius of the seed-photon emitting region is ∼10 km in the HB, similar to the radii of the seed-photon emitting region inferred for GX 17+2 and GX 349+2, while it decreases significantly in the NB, where it ranges from ∼1.8 km in the upper NB to ∼3.5 km in the lower NB. The radius of the seed-photon emitting region suggests that the NS itself (or the boundary layer between the accretion disk and the NS) could provide the soft photons which are then Comptonized in a surrounding cloud. The Comptonizing cloud might then be a hot corona, a hot flared inner disk, or even the boundary layer between the NS and the accretion disk if it is sufficiently thin and hot (as suggested by Popham & Sunyaev 2001).

However, in the NB of Cyg X–2 the seed-photon emitting radius becomes much smaller than the NS radius, although we note that the model we use is probably too simple to realistically describe the emission region in these systems, where gradients of temperature and other parameters are possible, if not probable. The smaller value of the seed-photon radius is due to the bolometric flux of the Comptonized component, which is lower by a factor of 2 with respect to that in the HB, and the seed-photon temperature, which is higher by a factor of 2.

A possibility to explain the small seed-photon radius in the NB of Cyg X–2 is that the geometry becomes nonspherical at some critical accretion rate. For instance, the fit results might be explained if at high accretion rates most of accreting plasma in the Comptonizing cloud collapses to a geometrically thin disk, leaving only an optically thin cloud around the inner part of the system, which can be responsible for the Comptonization. Because now the accretion occurs mostly onto the equator of the NS through the thin disk, the emitting region of soft seed-photons will be a strip at the NS equator, implying a reduced emitting area (a geometry similar to that proposed by Church & Balucinska-Church 1997). Correspondingly, because a similar (no more than a factor of two larger) amount of matter is accreted on a smaller area, the temperature of the NS blackbody emission, and therefore of the seed-photons for the Comptonization, increases. However, it is not clear why the accreting plasma should collapse to a geometrically thin disk at such high accretion rates. Another possibility to explain these changes is that some occulting material (e.g. from a flared inner disk) is obscuring the inner part of the Comptonizing region. In fact the absorption of the low energy part of the Comptonization spectrum might explain the reduction of the observed flux and the higher seed-photon temperature; the seed-photon temperature can be overestimated in this case, because it is mainly determined by the low energy cutoff in the Comptonization spectrum. Note that also the values we measure for the electron temperature and the optical depth may not be representative of the average properties of the Comptonizing region if we mostly see the emission from the outer part, which could have a lower optical depth and therefore a higher temperature. The fact that the Cyg-like Z sources (i.e. Cyg X–2, GX 5–1 and GX 340+0) are thought to have a higher inclination than the other Z sources (referred to as Sco-like sources; Kuulkers et al. 1994; Kuulkers & van der Klis 1995) might explain why in Cyg X–2 these changes are more pronounced than in GX 17+2.

A hard tail, which can be fitted by a power law with photon index ∼1.8–2, is significantly detected only in the HB spectra of Cyg X–2, and it is not required to fit the spectra in the NB. This behavior is similar to that observed (with much higher statistical significance, cf. Di Salvo et al. 2000) in GX 17+2, where a hard power-law tail was present in the HB spectra and weakened (by up to a factor of ∼20) when the source moved down the NB. This similarity is in agreement with the idea of a correlation between the radio flux, which is observed to have a maximum in the HB (Hasinger et al. 1990; Penninx et al. 1988), and the hard tail, which would imply that the hard power-law component is related to the high-velocity electrons (probably from a jet) producing the radio emission. Note also that the power-law component seems to be

weaker in Cyg X–2, where it contributes a lower fraction of the total luminosity, and, correspondingly, the radio emission is weaker (see e.g. Fender & Hendry 2000 and references therein). This might be explained by the high inclination of the source, if the radio and the hard X-ray emissions are produced by a jet which is collimated along the perpendicular to the disk.

Two (broad) emission lines are needed to fit the spectrum of Cyg X–2. The first one is detected at an energy around 1 keV, with a width of σ $\sim$0.1–0.2 keV and equivalent width between 30 and 80 eV. Both the width and the equivalent width of this line are significantly larger in the HB than in the NB. The LECS data of the 1996 BeppoSAX observation, when the source was in the HB, were already analyzed by Kuulkers et al. (1997). They found very similar parameters for this emission line, despite their somewhat different continuum model. This feature is probably due to blending of narrow emission lines, as testified to by the fact that the previous higher-resolution observations obtained with the Einstein Objective Grating Spectrometer (OGS) require the presence of multiple line emission around 1 keV from highly ionized Fe, O and other medium Z elements (Vrtilek et al. 1988). The other emission line is detected at an energy of 6.6−6.7 keV, compatible with Kα emission from highly ionized Fe. The width and equivalent width of this line are also variable, in the range 0.2–0.65 keV and 20–55 eV, respectively, without any clear correlation with the position of the source in the CD/HID. A broad ($FWHM \sim 1$ keV) Fe line at $\sim$6.7 keV, with an equivalent width of $\sim$60 eV, was measured in BBXRT data when the source was in a high state, on the lower part of the NB (Smale et al. 1993). These line parameters are very similar to the ones we measure in the lower NB spectrum. Smale et al. (1993) argue that this line can be produced by reflection from the inner accretion disk if the disk surface is highly ionized. Note that in this case the large width of the iron line is also in agreement with the idea that the source is observed at a high inclination angle. Other narrow emission/absorption features could be present in the low energy (below 5 keV) spectrum of Cyg X–2. In particular an emission line at $\sim$2.5 keV is detected with statistical significance. The energy of this line is consistent with Lyα emission from S XVI at 2.62 keV (see also Kuulkers et al. 1997).

5. Conclusions

We have reported on the results of a broad band (0.1–200 keV) spectral analysis of Cyg X–2 using two BeppoSAX observations taken in 1996 and 1997, respectively. The source was in the HB and NB during the 1996 and 1997 observation, respectively. In our spectral deconvolution, using a two-component continuum consisting of a disk blackbody and a Comptonization model, the transition from the HB to the NB can be ascribed to a variation of the soft blackbody component, which becomes harder (and broader) in the NB, and of the Comptonization component, which becomes less prominent in the NB. Based on these results, we interpret the soft blackbody component in the spectra of Z sources as the emission from the inner accretion disk, as previously proposed by the so-called Eastern model. The Comptonization component may then be emitted by hot plasma surrounding the NS. In this interpretation, the changes in the parameters of the soft component indicate that the inner rim of the disk approaches the NS surface when the source moves from the HB to the NB, i.e. as the (inferred) mass accretion rate increases. However, it is not clear why a similar behavior is not observed in other Z sources such as GX 17+2, where the soft component is not observed to change significantly as the source moves from the HB to the NB. The parameters of the Comptonized component in Cyg X–2 also change significantly when the source moves from the HB to the NB. These changes can be explained by an occultation of the Comptonizing region probably caused by matter in an inner flared disk, or by an evolution from a spherical to a non-spherical geometry of the Comptonizing cloud. Finally we report the presence of a hard power-law tail, which is significantly detected in the HB spectra, where it contributes $\sim$1.5% of the source luminosity. Although the relatively poor statistics does not allow a definitive conclusion, the hard tail might be weaker in the NB. This would be in agreement with the behavior shown by GX 17+2 and with the idea of a correlation between radio flux and hard X-ray tails.

Acknowledgements. This work was partially supported by the Netherlands Organization for Scientific Research (NWO).

References

Asai, K., Dotani, T., Mitsuda, K., et al. 1994, PASJ, 46, 479
Barret, D., Olive, J. F., Boirin L., et al. 2000, ApJ, 533, 329
Barret, D., Mereghetti, S., Roques, J. P., et al. 1991, ApJ, 379, L21
Boella, G., Butler, R. C., Perola, G. C., et al. 1997a, A&AS, 122, 299
Boella, G., Chiappetti, L., Conti, G., et al. 1997b, A&AS, 122, 327
Casares, J., Charles, P. A., & Kuulkers, E. 1998, ApJ, 493, L39
Churazov, E., Gilfanov, M., Sunyaev, R., et al. 1997, Adv. Space Res., 19, 55
Church, M. J., & Balucinska-Church, M. 2001, A&A, 369, 915
D'Amico, F., Heindl, W. A., Rothschild, R. E., & Gruber, D. E. 2001, ApJ, 547, L147
Di Salvo, T., Stella, L., Robba, N. R., et al. 2000, ApJ, 544, L119
Di Salvo, T., Robba, N. R., Iaria, R., et al. 2001, ApJ, 554, 49
Done, C., Zycki, P. T., & Smith, D. A. 2002, MNRAS, in press [astro-ph/0111497]
Fender, R. P., & Hendry, M. A. 2000, MNRAS, 317, 1
Frank, J., King, A., & Raine, D. 1992, Accretion Power in Astrophysics (Cambridge Astrophysics Ser. 21; Cambridge: Cambridge Univ. Press)
Frontera, F., Costa, E., Dal Fiume, D., et al. 1997, A&AS, 122, 357

Frontera, F., Dal Fiume, D., Malaguti, G., et al. 1998, Nuclear Phys. B (Proc. Suppl.), 69, 286
Harmon, B. A., Wilson, C. A., Tavani, M., et al. 1996, A&AS, 120, 197
Hasinger, G., & van der Klis, M. 1989, A&A, 225, 79
Hasinger, G., van der Klis, M., Ebisawa, K., Dotani, T., & Mitsuda, K. 1990, A&A, 235, 131
Hirano, A., Kitamoto, S., Yamada, T. T., Mineshige, S., & Fukue, J. 1995, ApJ, 446, 350
Hjellming, R. M., Han, X. H., Cordova, F. A., & Hasinger, G. 1990, A&A, 235, 147
Homan, J., van der Klis, M., Jonker, P. G., et al. 2002, ApJ, in press [astro-ph/0104323]
Hoshi, R., & Mitsuda, K. 1991, PASJ, 43, 485
Hua, X.-M., & Titarchuk, L. 1995, ApJ, 449, 188
Iaria, R., Burderi, L., Di Salvo, T., La Barbera, A., & Robba, N. R., 2001, ApJ, 547, 412
in 't Zand, J. J. M., Verbunt, F., Strohmayer, T. E., et al. 1999, A&A, 345, 100
Kahn, S. M., & Grindlay, J. E. 1984, ApJ, 281, 826
Kallman, T. R., Vrtilek, S. D., & Kahn, S. M. 1989, ApJ, 345, 498
Kuulkers, E., Parmar, A. N., Owens, A., Oosterbroek, T., & Lammers, U., 1997, A&A, 323, L29
Kuulkers, E., van der Klis, M., & Vaughan, B. A. 1996, A&A, 311, 197
Kuulkers, E., Homan, J., van der Klis, M., Lewin, W.H.G., & Méndez, M., 2002, A&A, 382, 947
Kuulkers, E., van der Klis, M., Oosterbroek, T., et al. 1994, A&A, 289, 795
Kuulkers, E., & van der Klis, M. 1995, A&A, 303, 801
Ling, J. C., Wheaton, W. A., Mahoney, W. A., et al. 1996, A&AS, 120C, 677
Manzo, G., Giarrusso, S., Santangelo, A., et al. 1997, A&AS, 122, 341
Markoff, S., Falcke, H., & Fender, R. 2001, A&A, 372, L25
Matt, G., Costa, E., dal Fiume, D., et al. 1990, ApJ, 355, 468
Maurer, G. S., Johnson, W. N., Kurfess, J. D., & Strickman, M. S. 1982, ApJ, 254, 271
Méndez, M. 2000, Proc. 19th Texas Symp. Relativistic Astrophysics and Cosmology, ed. J. Paul, T. Montmerle, & E. Aubourg (Amsterdam: Elsevier), 15
Mitsuda, K., Inoue, H., Koyama, K., et al. 1984, PASJ, 36, 741
Orosz, J. A., & Kuulkers, E. 1999, MNRAS, 305, 132
Parmar, A. N., Martin, D. D. E., Bavdaz, M., et al. 1997, A&AS, 122, 309
Penninx, W., Lewin, W. H. G., Zijlstra, A. A., Mitsuda, K., & van Paradijs, J. 1988, Nature, 336, 146
Peterson, L. E., & Jacobson, A. S. 1966, ApJ, 145, 962
Peterson, L. E. 1973, in X-ray and Gamma-ray Astronomy, ed. H. Bradt, & R. Giacconi, IAU Symp., 55, 51
Piraino, S., Santangelo, A., Ford, E. C., & Kaaret, P. 1999, A&A, 349, L77
Piraino, S., Santangelo, A., & Kaaret, P. 2002, ApJ, in press [astro-ph/0110553]
Popham, R., & Sunyaev, R. 2001, ApJ, 547, 355
Psaltis, D., Belloni, T., & van der Klis, M. 1999, ApJ, 520, 262
Shimura, T., & Takahara, F. 1995, ApJ, 445, 780
Smale, A. P., Done, C., Mushotzky, R. F., et al. 1993, ApJ, 410, 796
Strickman, M., & Barret, D. 2000, AIP Conf. Proc., 510, 222
Sunyaev, R. A., & Titarchuk, L. G. 1980, A&A, 86, 121
Titarchuk, L. 1994, ApJ, 434, 570
Titarchuk, L., & Lyubarskij, Y. 1995, ApJ, 450, 876
van der Klis, M. 2000, ARA&A, 38, 717
van der Klis, M. 2001, ApJ, 561, 943
van der Klis, M. 1995, in X-Ray Binaries, ed. W. H. G Lewin, J. van Paradijs, & E. P. J. van den Heuvel (Cambridge Astrophysics Series, Cambridge), 252
van Paradijs, J., & van der Klis, M. 1994, A&A, 281, L17
van Paradijs, J., Allington-Smith, J., Callanan, P., et al. 1990, A&A, 235, 156
Vrtilek, S. D., Raymond, J. C., Garcia, M. R., et al. 1990, A&A, 235, 162
Vrtilek, S. D., Swank, J. H., Kelley, R. L., & Kahn, S. M. 1988, ApJ, 329, 276
Vrtilek, S. D., Kahn, S. M., Grindlay, J. E., Seward, F. D., & Helfand, D. J. 1986, ApJ, 307, 698
Vrtilek, S. D., Penninx, W., Raymond, J. C., et al. 1991a, ApJ, 376, 278
Vrtilek, S. D., McClintock, J. E., Seward, F. D., Kahn, S. M., & Wargelin, B. J. 1991b, ApJS, 76, 1127
White, N. E., Peacock, A., Hasinger, G., et al. 1986, MNRAS, 218, 129
White, N. E., Stella, L., & Parmar, A. N. 1988, ApJ, 324, 363
Wijnands, R., & van der Klis, M. 1999, ApJ, 514, 939
Wijnands, R., Homan, J., van der Klis, M., et al. 1998, ApJ, 493, L87
Wijnands, R., Homan, J., van der Klis, M., et al. 1997, ApJ, 490, L157
Yoshida, K., Mitsuda, K., Ebisawa, K., et al. 1993, PASJ, 45, 605
Zhang, S. N., Cui, W., & Chen, W. 1997, ApJ, 482, L155